Theoretical and experimental study of the effects of spray inclination on two-phase spray cooling and critical heat flux

Milan Visaria, Issam Mudawar *

Boiling and Two-phase Flow Laboratory, School of Mechanical Engineering, Purdue University, West Lafayette, IN 47906, USA

Abstract

Experiments were conducted with PF-5052 liquid sprays impacting a $1.0 \times 1.0 \text{ cm}^2$ heated test surface at different inclination angles, flow rates, and subcoolings. Inclination angle had no noticeable effect on the single-phase or two-phase regions of the boiling curve. Maximum CHF was always achieved with the spray impinging normal to the test surface; increasing angle of inclination away from the normal decreased CHF appreciably. Video analysis showed inclined sprays produced lateral liquid film flow towards the farthest downstream region of the test surface. The film liquid provided partial resistance to dryout despite the weak volumetric spray flux in the downstream region. A new theoretical model of the spray's impact area and volumetric flux proves this decrease is the result of a sharp reduction in the fraction of the test surface area that is directly impacted by the spray. Combining the model and video results with a previous point-based CHF correlation for normal sprays is shown to accurately predict the effects of orientation angle on CHF for different nozzles and operating conditions.

1. Introduction

1.1. Background

Much of the early research on spray cooling concerns high-temperature applications found in materials processing. The past two decades, however, have witnessed considerable interest in the implementation of spray cooling in relatively low temperature applications involving the removal of high heat fluxes from small surfaces, such as electronics, avionics, lasers, and microwave defense systems [1–3]. While the desire to maintain low surface temperatures during high-flux heat removal is an obvious benefit to these applications, spray cooling provides the added benefit of temperature uniformity across the surface being cooled. Cooling effectiveness is achieved by breaking the liquid into fine droplets having large surface-area-to-

volume ratio, which are emitted in multiple directions, impacting most of the surface [1]. Those same attributes help delay the onset of critical heat flux (CHF) during nucleate boiling. Despite those advantages, spray cooling has not achieved widespread implementation in the intended applications because of relatively poor understanding of how key spray parameters influence cooling performance, and the lack of long-term repeatability of cooling performance due to both corrosion and erosion of intricate passages inside the spray nozzle [1].

A number of physical as well as geometrical parameters are known to influence the cooling performance of a spray. For a given nozzle type, cooling performance is influenced by fluid properties, pressure drop, and subcooling, which, in turn, affect flow rate, mean droplet diameter, droplet velocity, and volumetric flux. Geometrical parameters include cone angle, orifice-to-surface distance, surface shape and size, and spray inclination angle. As discussed below, the influences of the physical parameters have been researched for some time, while the importance of geometrical parameters has only recently been emphasized.

---

* Corresponding author. Tel.: +1 765 494 5705; fax: +1 765 494 0539.
 E-mail address: mudawar@ecn.purdue.edu (I. Mudawar).

Nomenclature

a	half-length of major axis of elliptical impact area		T_{sat}	saturation temperature based on test chamber pressure
A	area of test surface		$T_{s,m}$	test surface temperature at CHF
A'	area of spherical surface		ΔT_{sub}	difference between saturation temperature and inlet temperature, $T_{sat}-T_f$
A''	area of projected surface			
$A_{ellipse}$	area of impact ellipse		We_{d_o}	Weber number based on nozzle orifice diameter
b	half-length of minor axis of elliptical impact area		x	coordinate in plane of test surface
			y	coordinate in plane of test surface
c_p	specific heat			
d_o	diameter of nozzle orifice		*Greek symbols*	
d_{32}	Sauter mean diameter (SMD)		α	inclination angle between spray axis and normal to test surface
g	gravitational acceleration			
h_{fg}	latent heat of vaporization		β	angle used in uniform point source model (see Fig. 8)
H	radius of spherical surface (see Fig. 8)			
H_N	distance from orifice to test surface		γ	angle used in uniform point source model (see Fig. 9)
k	thermal conductivity			
L	length (and width) of square test surface		γ'	angle used in uniform point source model (see Fig. 9)
P	pressure			
ΔP	pressure drop across spray nozzle		θ	spray cone angle
Q	total volumetric flow rate of spray		μ	viscosity
Q''	local volumetric flux across test surface		ρ	density
$\tilde{q}''$	heat flux based on total area (L^2) of test surface		σ	surface tension
q''_m	critical heat flux based on total area (L^2) of test surface			
			Subscripts	
$q''_{m,p}$	point-based critical heat flux		f	liquid
Q''_{sp}	local volumetric flux across spherical surface		g	vapor
R	radius of projected surface (see Fig. 8)		m	maximum (CHF)
Re_{d_o}	Reynolds number based on nozzle orifice diameter		s	test surface
			sat	saturation
T_f	liquid temperature at nozzle inlet		sub	subcooled
T_s	test surface temperature			

Implementation of spray cooling in emerging electronics and aerospace applications requires both a fundamental understanding of how spray parameters influence cooling performance and simple correlations and/or models of cooling behavior. CHF is perhaps the most important design parameter for heat-flux-controlled surfaces because its magnitude sets an upper limit on the amount of heat that can be removed during the efficient nucleate boiling regime. Some researchers suggested that spray CHF be correlated relative to volumetric flux [4–9] and Sauter mean diameter (SMD), d_{32} [5–9]. Others suggested correlating CHF with mean droplet size and velocity [10,11]. Volumetric flux is the volume of liquid impacting the surface per unit area per unit time. It has units of velocity and accounts for the cumulative effect of spray droplets as they impact the surface. A key advantage to using volumetric flux as the characteristic velocity for a spray in CHF correlations is the ability of this parameter to account for cooling deficiency towards the outer periphery of the spray impact area. Mean droplet velocity, on the other hand, has nearly the same magnitude across the impact area and, therefore,

cannot account for this cooling deficiency. Furthermore, the orifice-to-surface distance, which has a substantial influence on CHF, also has a strong influence on volumetric flux but not mean droplet velocity [7]. Therefore, volumetric flux is highly effective at accounting for the observed CHF trends.

1.2. Geometrical considerations

Imposing stringent geometrical constraints is paramount to ensuring consistency and repeatability when performing spray-cooling experiments. Unfortunately, most published spray cooling studies fail to specify the orifice-to-surface distance or to indicate if such distance was preserved when comparing data for different flow rates or other operating conditions. For a given spray angle, the orifice-to-surface distance dictates the diameter of the spray's impact area. Mudawar and Estes [8] showed that maximum CHF is achieved when the spray in configured such that the impact area just inscribes a square test surface. Much smaller orifice-to-surface distances allow only

a small fraction of the test surface to be impacted by the spray, while very large distances cause a substantial fraction of the spray liquid to fall wastefully outside the test surface. Mudawar and Estes showed experimentally that CHF is quite small for both extremes. This trend alone shows the great importance of accurately accounting for geometrical parameters when developing a CHF model.

Not much published literature is available on the effects of spray inclination on two-phase cooling performance. In a recent study, Silk et al. [12] examined the effects of spray inclination using PF-5060 as working fluid and both flat and enhanced copper test surfaces. They tested sprays that were inclined 0°, 30°, and 45° with the normal to the surface while maintaining a constant orifice-to-surface distance; their heat flux was based on the projected area of the test surface. For both the flat and enhanced surfaces, they noted that maximum CHF was achieved at an inclination angle of 30°. This behavior was attributed to the sweeping motion of spray droplet's horizontal velocity component while maintaining a dominant vertical velocity component.

Unlike the vast majority of published studies, which concern sprays pointed normal to the test surface, the present study, like Silk et al.'s, will explore the variations in cooling performance as the inclination angle is increased from 0° (spray axis normal to surface) toward 90°. A new model is developed that predicts the spatial distribution of volumetric flux and impact area for an inclined spray whose impact area just inscribes the square test surface. This model is incorporated into an earlier point-based CHF correlation by Estes and Mudawar [7] to facilitate CHF determination for different inclination angles, flow rates, and subcoolings. Experiments were also performed using three full-cone spray nozzles and PF-5052 as working fluid. Each nozzle was tested at inclinations from 0 to 55° and two subcoolings. The experimental findings are used to both help ascertain the influence of impact pattern on CHF and validate the new CHF model.

2. Experimental methods

2.1. Flow loop

The experimental portion of the present study was performed using dielectric coolant PF-5052, a product of 3M™ Company. This coolant has a relatively low boiling point of 50 °C at 1 atm., which facilitates lower surface temperatures than other popular dielectric coolants such as Fluorinerts FC-72 (56 °C) and FC-77 (97 °C). Relevant properties of saturated PF-5052 at 1 atm. are as follows: $\rho_f = 1643$ kg/m^3, $\rho_g = 12.0$ kg/m^3, $\sigma = 0.013$ N/m, $h_{fg} = 104{,}700$ J/kg, $c_{p,f} = 1092$ J/kg K, $\mu_f = 517 \times 10^{-6}$ N s/m^2, and $k_f = 0.058$ W/m K.

The test heater was mounted at the bottom of a test chamber while the fluid was sprayed downwards at different inclination angles. As shown in Fig. 1, a closed two-phase loop was used to deliver PF-5052 liquid to the test chamber at the appropriate pressure, temperature and flow rate. The fluid was separated by gravity inside the test chamber; liquid drained to the lower portion of a large reservoir while the vapor was routed to the upper portion of the same reservoir. Below the reservoir was situated a deaeration chamber fitted with an immersion heater. Two magnetically coupled centrifugal pumps were connected in parallel to provide the require range of coolant flow rates. The pumped liquid passed through a filter followed by one of two parallel rotameters before entering a finned-tube heat exchanger, which was cooled by two
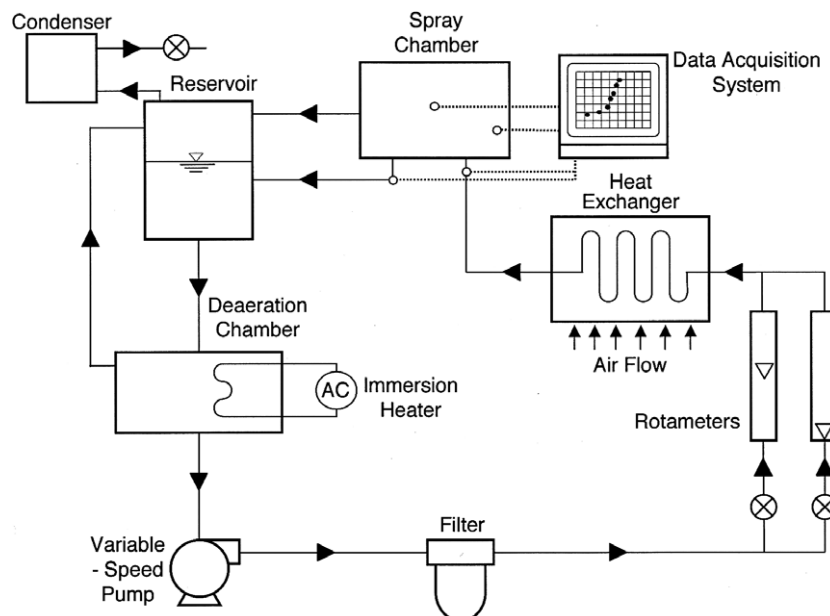
Fig. 1. Two-phase spray cooling loop.

high-capacity fans. The heat exchanger served as a pre-cooler that helped to set the subcooling of the liquid as it entered the spray nozzle. The vapor exiting the test chamber was routed first to the top portion of the reservoir and then into a finned-tube condenser where it was converted to liquid, which dripped back to the reservoir.

2.2. Nozzle positioning system

The test chamber itself was a tall rectangular enclosure made from G-10 fiberglass plastic. The test chamber was fitted with a front wall and a side window made from transparent polycarbonate plastic. A thermocouple and a pressure sensor were placed in the test chamber to measure the chamber's inside temperature and pressure, respectively.

Fig. 2 shows a translation/rotation platform that was used to set the position of the spray nozzle relative to the test surface inside the test chamber. The orifice-to-surface distance was adjusted with the aid of a vertical translation stage that was attached to two vertical aluminum rods; vertical motion was controlled by an external micrometer. A second, horizontal translation stage was mounted in a rectangular groove in the vertical stage. A small scale was glued to the horizontal stage to aid in manual positioning of this stage. Attached to the horizontal stage was a third, angular stage. A series of holes in the rotation stage spanned 0–90° from normal in 5° increments. The spray nozzle itself was mounted to a bracket that was attached to the rotation stage. The bracket was attached both at the center of rotation as well as with a pin that traversed the bracket to one of the holes in the angular stage; the pin position set the inclination angle of the nozzle.

2.3. Test heater

As shown in Fig. 3a, the 1.0×1.0 cm^2 test surface consisted of a square platform that protruded vertically upwards from a larger oxygen-free copper block. The underside of the copper block was bored to accept nine 220 W cartridge heaters. To minimize heat loss, all surfaces of the copper block were insulated except the test surface. A type-K (Chromel–Alumel) thermocouple was embedded 1.27 mm below the test surface to measure the surface temperature, accounting for the temperature gradient between the thermocouple bead and the surface. The test surface and surrounding G-7 insulation protruded slightly above the base of the test chamber to avoid any liquid accumulation above the test surface.

2.4. Operating procedure

The experiments were performed using three Unijet full-cone nozzles made by Spraying Systems Company. Key hydrodynamic characteristics of these sprays are listed in Table 1. Preparations for tests commenced by attaching a nozzle to the angular stage and adjusting the nozzle positioning system to yield the desired orientation as shown in Fig. 2. The coolant was then poured into the reservoir. To deaerate the fluid, electrical power to the cartridge heater inside the deaeration chamber was increased to bring the fluid to a vigorous boil for about 30 min. During this time, a mixture of PF-5052 vapor and non-condensable
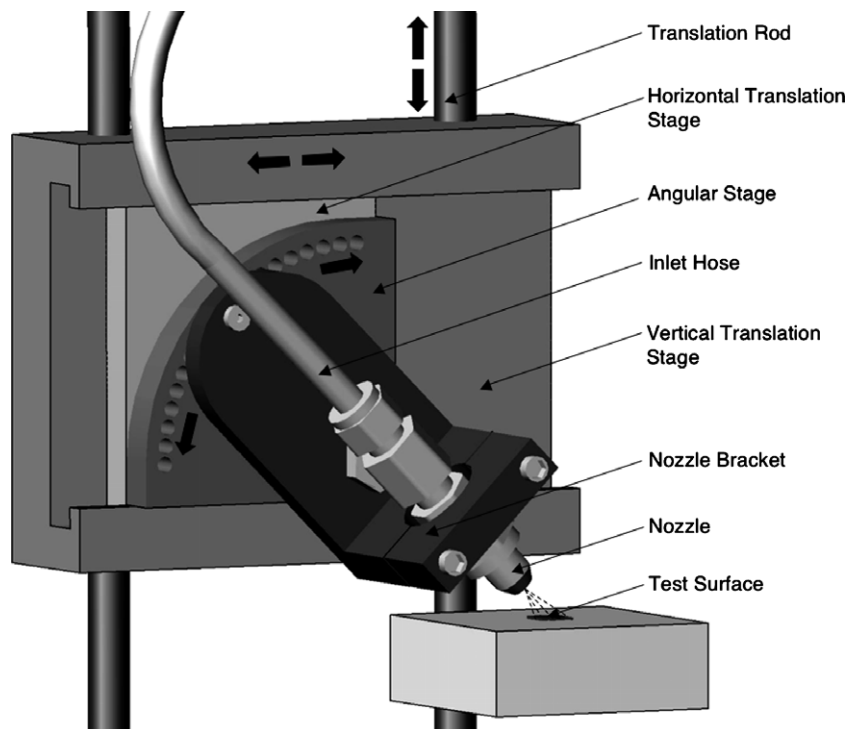
Fig. 2. Nozzle positioning system inside spray chamber.
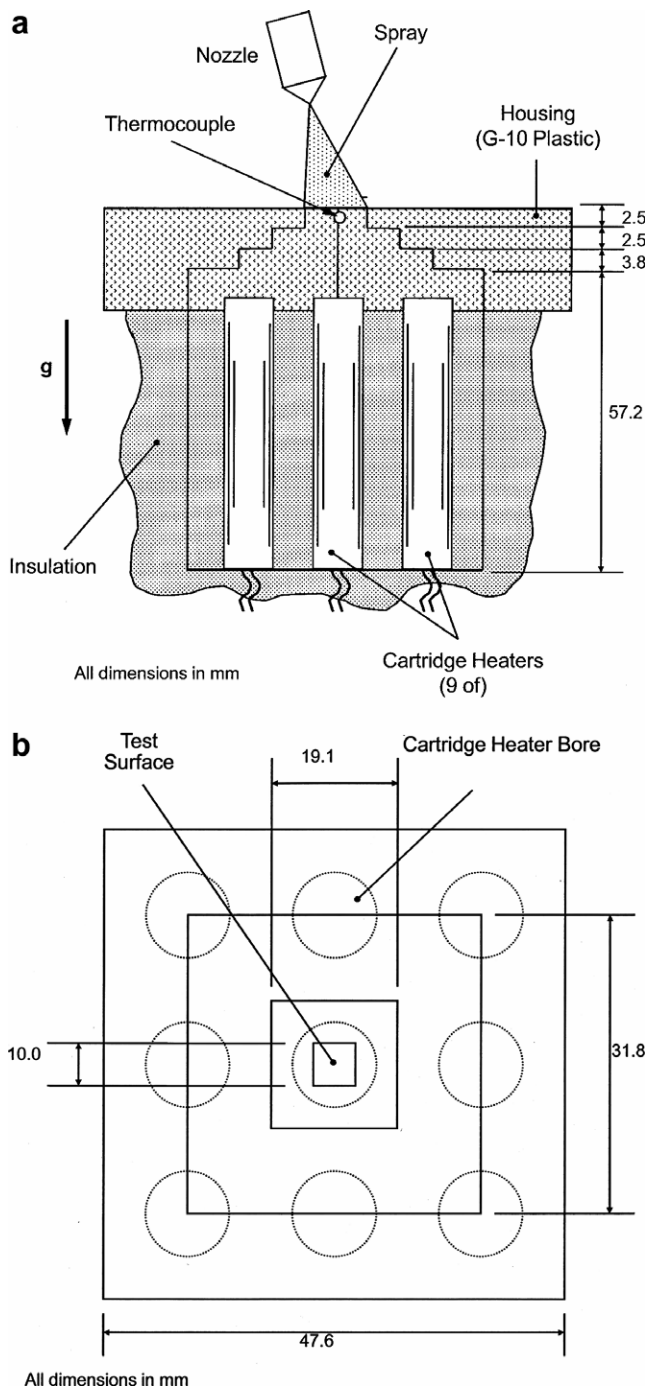
Fig. 3. (a) Sectional view of heater assembly and (b) top view of copper block.

Table 1
Characteristics of spray nozzles utilized in present study

Nozzle	Orifice diameter d_o (mm)	Spray Angle $(\theta°)$	Sauter mean diameter $d_{32} \times 10^6$ (m)	Volumetric flow rate $Q \times 10^6$ (m³ s⁻¹)
1	0.762	55.8	111–123	3.50–3.86
2	1.19	46.4	160–179	4.97–13.4
3	1.70	48.5	189–249	17.02

gases rose upwards to the reservoir followed by the condenser, where the vapor was recovered while the non-con-

densable gases were purged to the ambient through a vent. The pumps were then turned on and deaeration continued as the coolant circulated through the loop for 15 min. At the end of deaeration, the condenser vent was closed to completely isolate the loop fluid from the ambient. The pump power was then adjusted to provide the desired spray flow rate. The immersion heater was now used to pre-heat the fluid during tests requiring spray inlet temperatures exceeding ambient temperature. The spray temperature was fine-tuned with the aid of the finned-tube heat exchanger. Pressure inside the chamber was maintained at atmospheric level at all times. Sensors placed in the tube leading to the spray nozzle measured the inlet temperature and pressure while the outlet temperature and pressure were measured by sensors placed in the liquid tube exiting the spray chamber. Uncertainties in the pressure, flow rate and temperature measurements were less than 0.5%, 1.0% and ±0.2 °C, respectively.

Once the required operating conditions were achieved, electrical power was supplied to the copper block's cartridge heaters by a variable voltage transformer. The power input was measured with 0.5% accuracy Yokogawa digital wattmeter. Thermal analysis showed that less than 2% of the power input was lost to the ambient. Heat flux results were therefore based on electrical power input divided by the 1.0×1.0 cm² area of the test surface. A three-dimensional heat diffusion model using FLUENT showed that the surface temperature was very close to that inferred using one-dimensional heat conduction between the planes of the thermocouple and the test surface. The assumption of one-dimensional conduction was therefore used to determine test surface temperature throughout the study. The largest difference between surface temperatures using the two methods was 3.2 °C, corresponding to very low heat fluxes encountered in the single-phase region.

Unlike a normal spray, whose impact area is a circle, an inclined spray produces an elliptical impact area. To achieve the highest possible CHF for every inclination angle, all tests were performed with the major axis of the elliptical impact area just inscribing the square test surface. This important constraint will be discussed in detail in a later section.

Boiling curves were generated by increasing voltage across the cartridge heaters in small increments. Boiling data were recorded after steady-state was reached following each increment. As CHF neared, smaller voltage increments were used to refine CHF detection. At CHF, there was an unsteady rise in the heater temperature, which prompted the operator to abruptly turn off the electrical power input to preclude any physical damage to the heater parts.

3. Results and discussion

3.1. Boiling curves

Experiments were performed and boiling curves generated for PF-5052 at 1 atm using three different full-cone

spray nozzles. The nozzles are designated in Table 1 as 1, 2 and 3 in order of increasing flow capacity. The flow rates were varied from $Q = 3.5 \times 10^{-6}$ to $1.7 \times 10^{-5} \, \text{m}^3/\text{s}$ for subcoolings of $\Delta T_{sub} = 25$ and 35 °C. For each set of flow conditions, tests were repeated at inclination angles of $\alpha = 0°, 10°, 25°, 40°$ and 55°, measured between the spray axis and the normal to the test surface (i.e., 0° corresponds to a spray impacting normal to the test surface).

Fig. 4a–c shows boiling curves for nozzles 1, 2 and 3, respectively, corresponding to 25 °C subcooling and five inclination angles. The flow rate is held constant for each nozzle to isolate the effects of inclination angle. Overall, there are only minor variations in both the single-phase and nucleate boiling regions with inclination angle, but the effect is very pronounced at CHF. CHF decreased

monotonically with increasing inclination angle. Comparing Fig. 4a–c shows increasing flow rate for any inclination angle delayed both the onset of boiling and CHF.

Fig. 5a–c shows similar boiling curves obtained at 15 °C subcooling. Here again, there are no appreciable changes in the single phase or nucleate boiling regions with inclination angle, but CHF did decrease monotonically with increasing inclination angle. Despite this decrease, it took longer time at larger inclination angles for the test surface to reach steady-state between power increments. Comparing Fig. 5a–c reveals the aforementioned trend of delayed onset of nucleate boiling and CHF with increasing flow rate for all inclination angles. Comparing Figs. 4 and 5 shows increasing subcooling also delays both the onset of boiling and CHF.
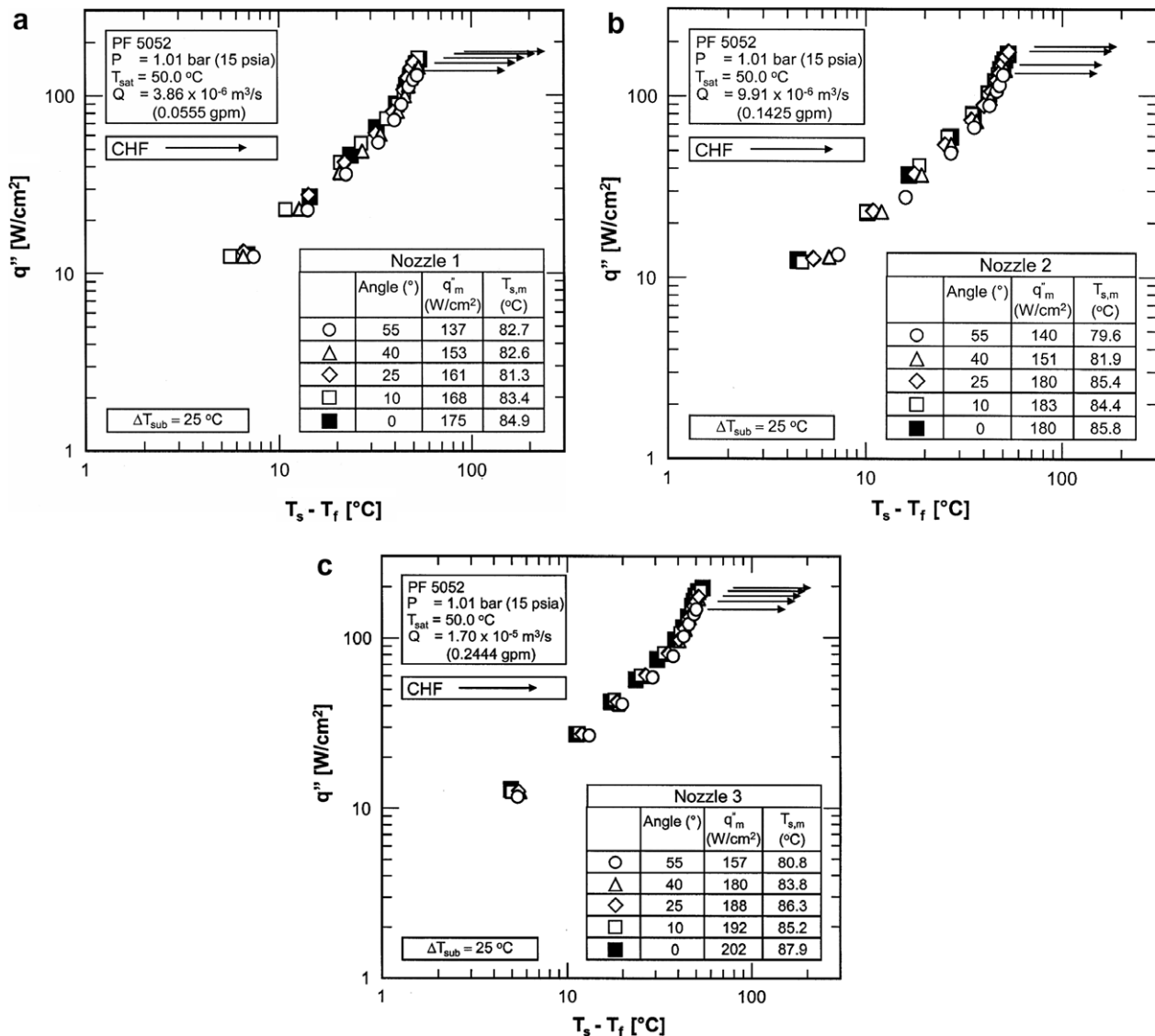
Fig. 4. Boiling curves for different inclination angles at 25 °C subcooling for: (a) nozzle 1 at $Q = 3.86 \times 10^{-6} \, \text{m}^3/\text{s}$, (b) nozzle 2 at $Q = 9.91 \times 10^{-6} \, \text{m}^3/\text{s}$, and (c) nozzle 3 at $Q = 1.70 \times 10^{-5} \, \text{m}^3/\text{s}$.
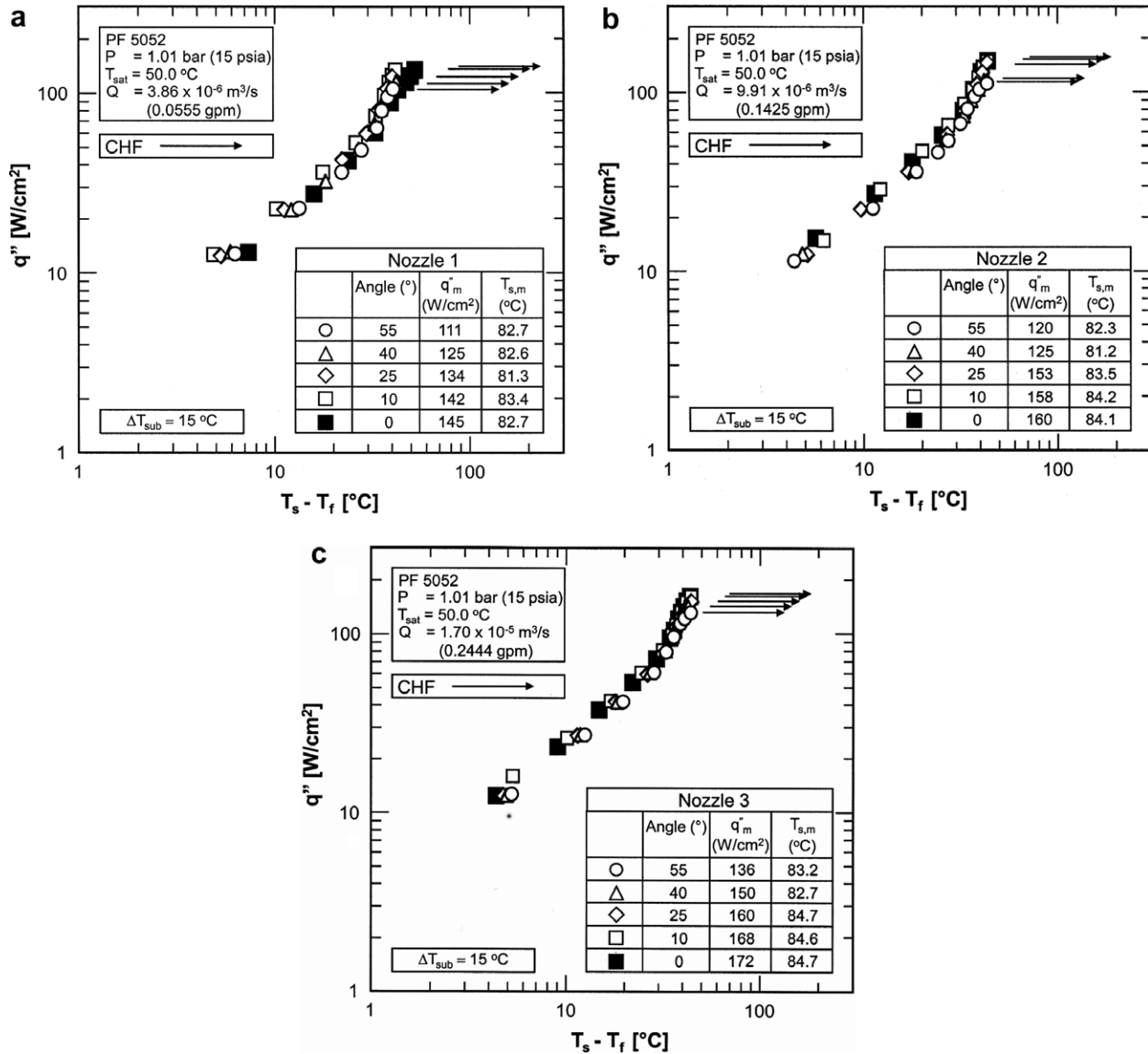
Fig. 5. Boiling curves for different inclination angles at 15 °C subcooling for: (a) nozzle 1 at $Q = 3.86 \times 10^{-6}$ m^3/s, (b) nozzle 2 at $Q = 9.91 \times 10^{-6}$ m^3/s, and (c) nozzle 3 at $Q = 1.70 \times 10^{-5}$ m^3/s.

3.2. CHF results

As indicated in the previous section, CHF increased with increases in flow rate and/or subcooling. Maximum CHF was achieved for every nozzle, flow rate and subcooling at 0° inclination, i.e., with the spray impacting normal to the test heater. CHF decreased with increasing inclination angle, reaching a minimum at the largest angle tested.

Following a previous model by Mudawar and Estes [8] for normal sprays, CHF was highest when the orifice-to-surface distance was adjusted such that the spray impact area just inscribed the 1.0×1.0 cm^2 test surface. Moving the nozzle close to the test surface causes all the liquid to impact a small portion of the test surface, depriving much of the surface of direct droplet impact. On the other hand, moving the nozzle far away from the test surface causes

much of the spray liquid to fall wastefully outside of the test surface. Mudawar and Estes showed both extremes yield low CHF values.

When the spray is inclined relative to the normal to the test surface, the impact area is an ellipse. To conform as closely as possible to the Mudawar and Estes criterion of a spray impact area just inscribing the test surface, all inclined nozzle tests in the present study were obtained with the major axis of the elliptical spray impact area just inscribing the square test surface. Under this constraint, increasing the inclination angle causes a pronounced decrease in both the length of the minor axis and the area of the impact ellipse, as illustrated in Fig. 6. Increasing inclination angle therefore causes a sharp reduction in the fraction of the test surface that is directly impacted by the spray droplets. However, there is a limit to the
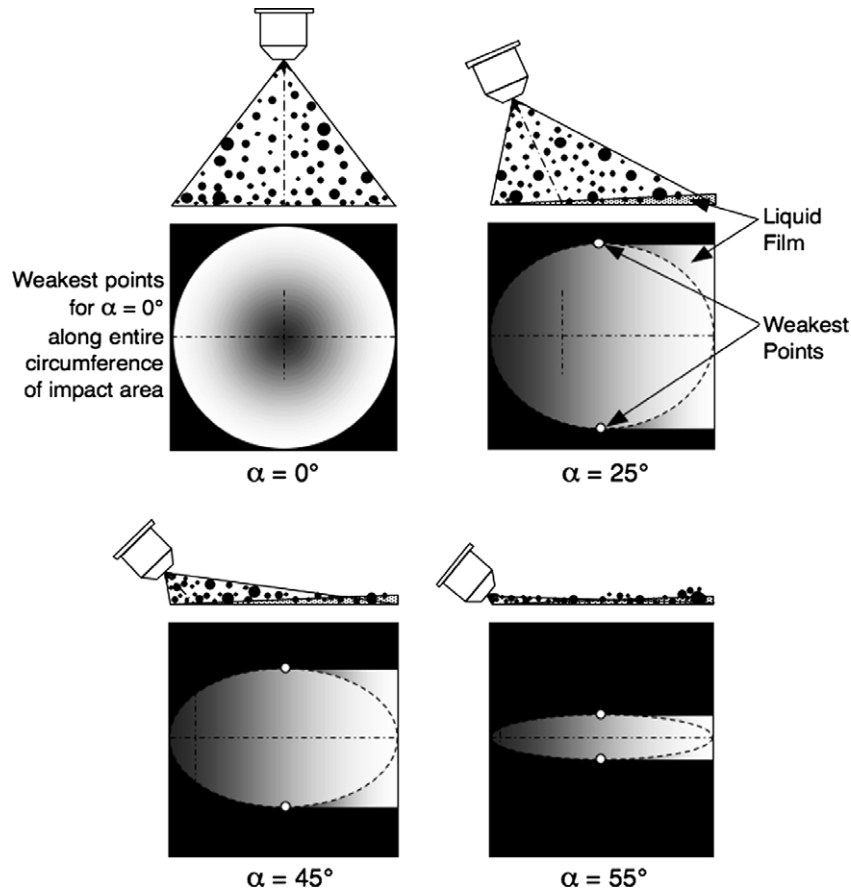
Fig. 6. Schematic representation of spray impact patterns for different inclination angles.

angle to which a spray can be inclined. This limit is given by

$$\alpha + \theta/2 \leqslant 90°. \tag{1}$$

Above this limit, no impact area can be formed. Fig. 6 shows how increasing spray inclination angle while keeping the spray impact area inscribed within the test surface requires the orifice-to-surface distance to be reduced. This causes the average volumetric flux across the test surface to increase but the local volumetric flux at the farthest downstream point to decrease.

As indicated in [7], CHF for a normal spray ($\alpha = 0°$) commences along the region of the test surface receiving the smallest volumetric, i.e., the outer periphery of the impact area. The situation is far more complicated for an inclined spray. Here, volumetric flux is smallest for points of the impact area that are farthest from the nozzle orifice.
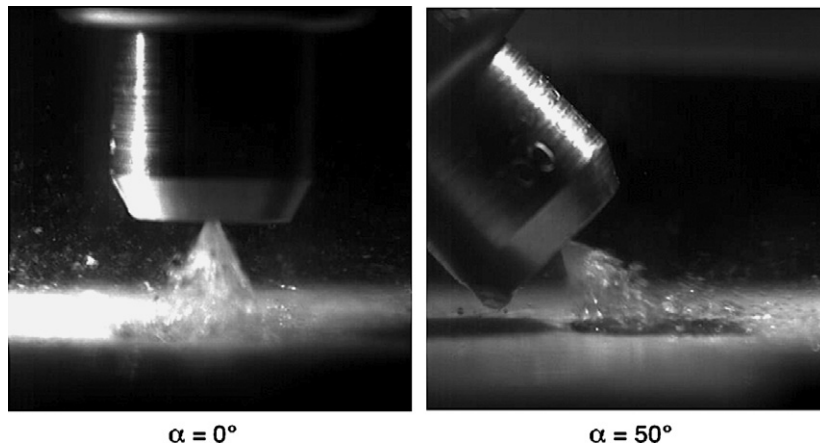
Fig. 7. Images of nozzle 1 adiabatic spray impact at $Q = 31.5 \times 10^{-6}$ m^3/s for two inclination angles.

Intuitively, one might conclude that the weakest point is the downstream outermost point of the major axis. Observation and video analysis showed otherwise. Fig. 7 shows still images of sprays impacting the surface adiabatically for $\alpha = 0$ and $50°$. Notice how the fluid is distributed uniformly at $0°$. However, there is significant lateral flow along the surface towards the farthest point for $\alpha = 50°$, increasing liquid flow along the entire surface downstream. The increased flow took the form of both droplets flowing nearly parallel to test surface, and a thin liquid film flowing along the test surface itself. As illustrated in Fig. 6, the weakest points for all inclination angles other than $\alpha = 0°$ are the end points of the minor axis, because these points are the farthest points from the orifice that do not benefit from the lateral liquid flow. It is therefore postulated that it is at these points where CHF commences first.

4. Volumetric flux model

In this section, a new analytical model is constructed to determine relations between the various geometrical parameters of an inclined spray. Earlier studies [5–9] showed that local volumetric flux, Q'', and Sauter mean diameter, d_{32}, are the two key hydrodynamic parameters that govern spray cooling performance and CHF. Estes and Mudawar [7] provided a correlation for d_{32} specifically tailored to the type of nozzle used in the present study; this diameter is fairly constant across the spray impact area. On the other hand, volumetric flux varies throughout the impact area. Therefore, what is needed for CHF determination for an inclined spray is a method for accurate determination of volumetric flux distribution across the test surface.

Estes and Mudawar [7] determined the volumetric flux distribution for a normal spray by assuming that the spray orifice represents a uniform point source for the sprayed fluid, i.e., the total spray flow rate Q is uniformly distributed across a spherical surface centered at the spray orifice and bounded by the spray cone angle θ. However, as will be explained below, the volumetric flux across the heater surface is not uniform.

Fig. 8 shows a geometrical model for an inclined spray. Like the Estes and Mudawar model, the orifice of the nozzle represents a point source for the sprayed liquid. Different surfaces are shown, whose relation to one another dictates the distribution of volumetric flux across test surface A. The first is spherical surface A' of radius H, which is the locus of points that are equidistant from the orifice. Volumetric flux is constant everywhere across spherical surface A' but is projected non-uniformly along an imaginary surface A'' perpendicular to the axis of the spray, decreasing radially outward from the orifice. The spray fluid traversing a differential area dA' of the spherical surface is projected first onto dA'' and then dA of the test surface. The volumetric flux, Q'', for dA is smaller than for dA'. Furthermore, Q'' is not constant along A, but decreases with increasing distance from the orifice.

The differential area dA' of the spherical surface is given by

$$dA' = 2\pi H^2 \sin \beta \, d\beta. \tag{2}$$

Integrating β between 0 and $\theta/2$ gives the area of the spherical surface bounded by the spray cone angle θ,

$$A' = 2\pi H^2 [1 - \cos(\theta/2)]. \tag{3}$$
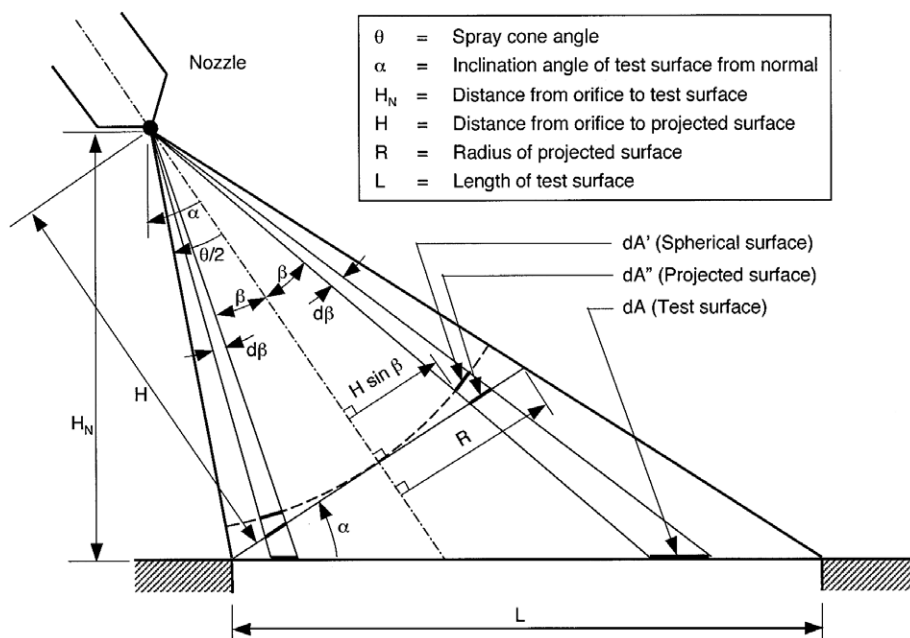
Fig. 8. Nomenclature for inclined spray model.

Since the spray flow rate is uniformly distributed across this spherical area, the volumetric flux for spherical surface A' is given by

$$Q''_{sp} = \frac{Q}{2\pi H^2 [1 - \cos(\theta/2)]}. \tag{4}$$

The volumetric flux across the test surface is given by

$$Q'' = Q''_{sp} \frac{dA'}{dA}. \tag{5}$$

Distance H is related to length L of the test surface by the relation

$$H = \frac{L}{2} [\cos\alpha \cot(\theta/2) - \sin\alpha]. \tag{6}$$

As illustrated in Fig. 9, an inclined spray produces an elliptical impact area on the test surface whose major axis ($2a$) is set equal to the heater length as discussed earlier.

$$2a = L. \tag{7}$$

The minor axis ($2b$) of the ellipse is given by

$$2b = L\cos\alpha \sqrt{1 - \tan^2\alpha \tan^2(\theta/2)}. \tag{8}$$

Eq. (8) indicates that the minor axis of the elliptical impact area decreases with increasing inclination angle α. The equation of the ellipse is

$$\frac{[x - (L/2)\tan\alpha \tan(\theta/2)]^2}{a^2} + \frac{y^2}{b^2} = 1, \tag{9}$$

and its area is given by

$$A_{\text{Ellipse}} = \frac{\pi}{4} L^2 \cos\alpha \sqrt{1 - \tan^2\alpha \tan^2(\theta/2)}. \tag{10}$$

Eq. (9) shows that the distance between the center of the heater and the spray axis increases with increasing α. Therefore, the horizontal position of the nozzle has to be adjusted for each inclination angle in order to inscribe the elliptical impact area (along the major axis) within the square test surface. Eq. (10) shows that the impact area is greatest for $\alpha = 0°$ and decreases monotonically with increasing α. Fig. 10 shows computed impact patterns for nozzle 1 corresponding to different inclination angles.

5. CHF model

Estes and Mudawar [7] developed a correlation for Sauter mean diameter (SMD) using the same three full-cone spray nozzles used in the present study and three different working fluids: water, FC-72, and FC-87.

$$\frac{d_{32}}{d_o} = 3.67 \left[We_{d_o}^{1/2} Re_{d_o} \right]^{-0.259}, \tag{11}$$

where We_{d_o} and Re_{d_o} are defined, respectively, as

$$We_{d_o} = \frac{\rho_g (2\Delta P/\rho_f) d_o}{\sigma}. \tag{12}$$

and

$$Re_{d_o} = \frac{\rho_f (2\Delta P/\rho_f)^{1/2} d_o}{\mu_f}, \tag{13}$$

ΔP is the pressure drop across the nozzle, and d_o the orifice diameter.

Estes and Mudawar also developed a correlation for point-based CHF, $q''_{m,p}$, along the outer periphery of the impact area for a normal spray using their own data for
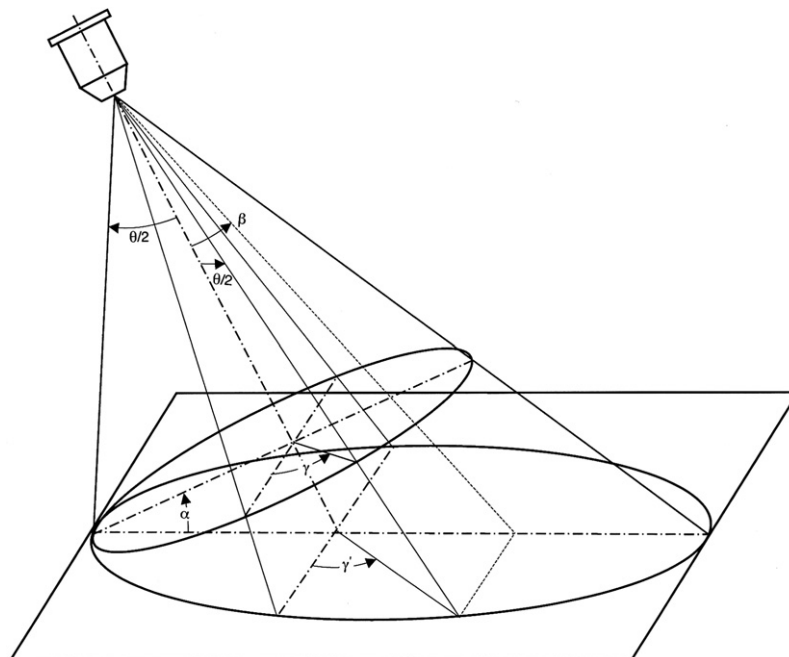
Fig. 9. Nomenclature for angles used in inclined spray model.
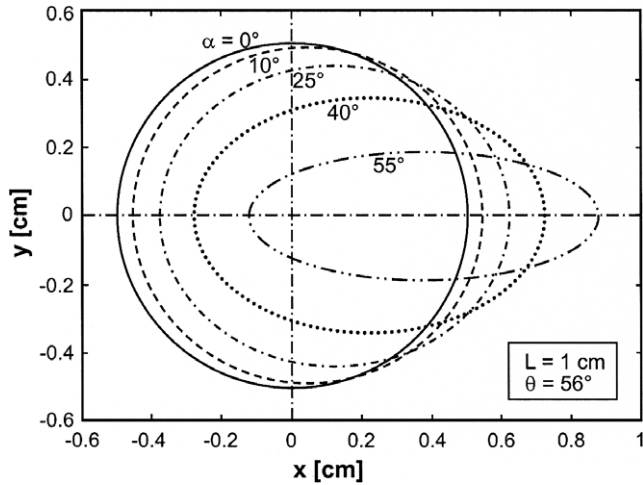
Fig. 10. Predicted variations of nozzle 1 spray impact area with inclination angle.

FC-72 and FC-87, along with water data obtained earlier by Mudawar and Valentine [5].

$$\frac{q''_{m,p}}{\rho_g h_{fg} Q''} = 2.3 \left(\frac{\rho_f}{\rho_g}\right)^{0.3} \left(\frac{\rho_f Q''^2 d_{32}}{\sigma}\right)^{-0.35} \left(1 + 0.0019 \frac{\rho_f c_{p,f} \Delta T_{sub}}{\rho_g h_{fg}}\right),$$

(14)

where Q'' is the local volumetric flux along the outer periphery of the impact area. Recently, Rybicki and Mudawar [9] validated this correlation for upward-oriented PF-5052 sprays as well.

As discussed earlier, inclining the spray relative to the normal to the test surface causes lateral liquid flow towards the farthermost downstream edge of the impact area. This phenomenon tends to overcome localized dryout in that region despite its low volumetric flux. On the other hand,

the end points of the minor axis of the impact ellipse are the farthest points from the orifice that do not benefit from the lateral liquid flow. Therefore Eq. (14) should be based on the value of Q'' at these two points.

As discussed in [7], local dryout reduces the fraction of the test surface area available for cooling and increases the heat flux within the impact area, enabling the dryout region to propagate inwards in an unstable manner. Therefore, CHF based on the total area of the test surface can be related to the point-based CHF by

$$q''_m = \frac{A_{Ellipse} q''_{m,p}}{L^2} = \left[\frac{\pi}{4} \cos\alpha \sqrt{1 - \tan^2\alpha \tan^2(\theta/2)}\right] q''_{m,p}.$$

(15)

To calculate $q''_{m,p}$ using Eq. (14), Q'' was determined by finding the flow rate of spray liquid impacting an infinitesimal differential area at either end of the minor axis. This was accomplished by first projecting an infinitesimal spherical surface area dA' at the location corresponding to the end points of the minor axis on the projection surface to determine dA'' for that location (see Fig. 8). This was followed by projecting dA'' on the test surface to determine dA. This entire process was performed numerically. Finally, Q'' for the end points of the minor axis was calculated using Eqs. (4) and (5).

Fig. 11 shows excellent agreement between the CHF model predictions and experimental data for the three nozzles for different subcoolings, flow rates and inclination angles. Virtually all the data fall within ±25% of the predictions with a mean absolute error of 9.04%. Fig. 12 shows the new model successfully predicts the effects of inclination angle on CHF for the individual nozzles. Notice the aforementioned monotonic decrease in both CHF data and the model predictions from a maximum corresponding to $\alpha = 0°$.
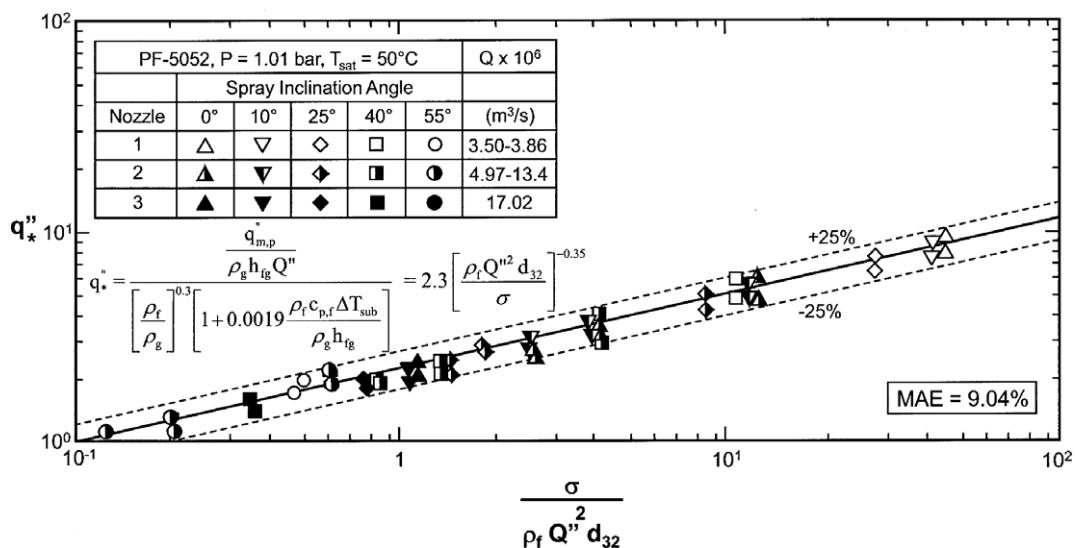
Fig. 11. Correlation of CHF data based on volumetric flux at weakest point of impact area for different nozzles, flow rates, subcoolings, and inclination angles.
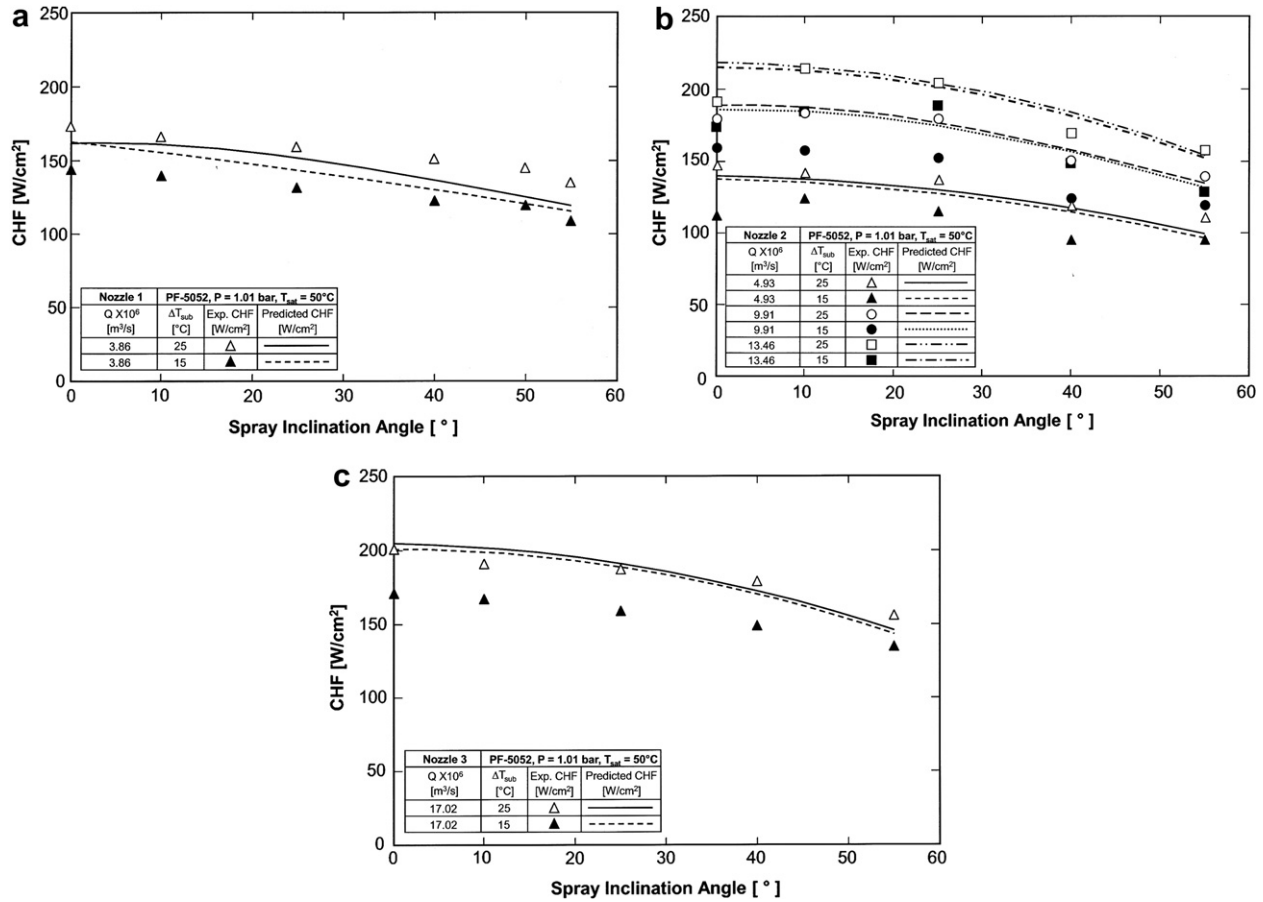
Fig. 12. Comparison of model predictions and experimental data for different inclination angles for: (a) nozzle 1, (b) nozzle 2, and (c) nozzle 3.

6. Conclusions

This study examined the effects of inclination angle of a spray on two-phase cooling performance. A new theoretical model was constructed to determine the shape and size of the spray impact as well as the distribution of volumetric flux across the test surface. Experiments were also performed using coolant PF-5052 for three full-cone spray nozzles at different flow rates, subcoolings, and inclination angles. The results of both the theoretical model and video analysis of the spray were used to construct a CHF model for inclined sprays. Key findings from the study are as follows.

1. Inclination angle has little effect on the single-phase and nucleate boiling regions of the boiling curve. However, CHF decreases appreciably with increasing inclination angle.
2. The impact area for an inclined spray impinging on a flat surface is an ellipse whose area decreases rapidly with increasing inclination angle.
3. Aside from the elliptical area incurring direct impact by the spray droplets, inclined sprays cause lateral liquid flow along the test surface in the form of a liquid film traveling towards the downstream region of the surface.

This liquid appears to partially compensate for weak volumetric flux and resist dryout in the downstream region.

4. While the lowest volumetric flux is encountered along the farthest downstream point of the impact area, CHF commences along the end points of the minor axis of the impact ellipse. These are the farthest points from the orifice that do not benefit from the lateral film flow.
5. Combining the new impact area and volumetric flux model with a previous correlation by Estes and Mudawar [7] provides an accurate means for predicting the effects of inclination angle on CHF.

References

[1] I. Mudawar, Assessment of high-heat-flux thermal management schemes, IEEE Trans.-CPMT: Compon. Packag. Technol. 24 (2001) 122–141.
[2] L. Lin, R. Ponnappan, Heat transfer characteristics of spray cooling in a closed loop, Int. J. Heat Mass Transfer 46 (2003) 3737–3746.
[3] D.P. Rini, R.-H. Chen, L.C. Chow, Bubble behavior and nucleate boiling heat transfer in saturated FC-72 spray cooling, J. Heat Transfer 124 (2002) 63–72.
[4] S. Toda, A study in mist cooling (1st report: investigation of mist cooling), Trans. Jap. Soc. Mech. Eng. 38 (1972) 581–588.
[5] I. Mudawar, W.S. Valentine, Determination of the local quench curve for spray-cooled metallic surfaces, J. Heat Treat. 7 (1989) 107–121.

[6] I. Mudawar, T.A. Deiters, A universal approach to predicting temperature response of metallic parts to spray quenching, Int. J. Heat Mass Transfer 37 (1994) 347–362.

[7] K.A. Estes, I. Mudawar, Correlation of Sauter mean diameter and critical heat flux for spray cooling of small surfaces, Int. J. Heat Mass Transfer 38 (1995) 2985–2996.

[8] I. Mudawar, K.A. Estes, Optimization and predicting CHF in spray cooling of a square surface, J. Heat Transfer 118 (1996) 672–680.

[9] J.R. Rybicki, I. Mudawar, Single-phase and two-phase cooling characteristics of upward-facing and downward-facing sprays, Int. J. Heat Mass Transfer 49 (2006) 5–16.

[10] C.S.K. Cho, K. Wu, Comparison of burnout characteristics in jet impingement cooling and spray cooling, in: Proceedings of the National Heat Transfer Conference, vol. 1, Houston, Texas, 1988, pp. 561–567.

[11] R.-H. Chen, L.C. Chow, J.E. Navedo, Effects of spray characteristics on critical heat flux in subcooled water spray cooling, Int. J. Heat Mass Transfer 45 (2002) 4033–4043.

[12] E.A. Silk, J. Kim, K. Kiger, 2005, Effect of spray cooling trajectory on heat flux for a straight finned enhanced surface, in: Proceedings of the National Heat Transfer Summer Conference, Paper HT2005-72634, San Francisco, CA, 2005.